Ceramics International 44 (2018) 22467–22472

Contents lists available at ScienceDirect

Ceramics International

journal homepage: www.elsevier.com/locate/ceramint

Optical properties of Er^{3+}/Yb^{3+} co-doped phosphate glass system for NIR lasers and fiber amplifiers

Yin Zhang[a,b,*], Mingming Li[a], Jun Li[a], Jun Tang[a], Weijing Cao[a], Zhenning Wu[a]

[a] College of Materials Science and Engineering, Nanjing Tech University, Nanjing 210009, China
[b] Nanjing Haoqi Advanced Materials Co., Ltd., Nanjing 211300, China

ARTICLE INFO

Keywords:
Phosphate glass
Rare earth doping
Optical properties
Judd-Ofelt parameters

ABSTRACT

In this research, the optical properties of Er^{3+}/Yb^{3+} co-doped phosphate glass have been studied to explore the potential of this glass system in laser and electronic amplifiers. The Judd–Ofelt (J-O) intensity parameter (Ω_t) in the J-O model was established to determine the absorption intensity of the glass. The optical properties of the glass can be evaluated by various radiation parameters such as the radiative transition probabilities (A_{rad}), stimulated emission cross sections (σ_e), branching ratios ($\beta_{JJ'}$), maximum half-width values ($\Delta\lambda_p$), and the radiation lifetime (τ_{rad}) of the glass. It was found that in the case of Yb^{3+} as a sensitizer, the spectral properties of the Er^{3+} doped glass can be maximized. The data of A_{rad}, $\beta_{JJ'}$, τ_{rad}, σ_e and $\Delta\lambda_p$ obtained by Er^{3+}/Yb^{3+} co-doping can find that the Er^{3+}-doped sample undergoes $^4I_{13/2}$–$^4I_{15/2}$ transition at 1.56 μm, and the stimulated emission cross section is greatly improved. The application prospects of the glass in solid near-infrared laser and electronic communication was discussed. According to the comprehensive discussion and analysis, the glass has great application potential.

1. Introduction

Nowadays, rare earth ion doped glasses have been widely studied due to their excellent optical properties to meet the application requirements in solid-state lasers, optical amplifiers and three-dimensional displays [1]. Recently, in order to meet the requirements for materials in optical data transmission, detection, sensing and laser technology, phosphate glass has attracted attention due to its unique properties [2]. Compared with silicate, borate and other glass hosts, phosphate glass has unique characteristics, including low melting point, high transparency, high gain density due to high solubility of lanthanide (Ln) ions, high thermal stability, low refractive index and low dispersion [3].

In rare earth ions, Er^{3+} and Yb^{3+} ions are more frequently focused. The emission of Er^{3+} at 1530 nm has attracted special attention in telecommunication applications. Because it is in the third fiber optic communication window [4]. This emission is critical for information transfer in Er^{3+} doped fiber optical amplifiers and is often used in wavelength division multiplexing networks [2]. Although in recent years the most part of the commercial fiber optical amplifiers are made of silicate glass in a communications network, it has a very narrow bandwidth emission at 1530 nm that limits its use in broadband applications. Therefore, the need to find more efficient fiber amplifiers and flat gain spectra led to explore more new glasses. In particular, the Er^{3+}-doped phosphate, bismuthate and tellurite glasses, which are of interest because of their large stimulated emission cross section and a wide fluorescent band at 1530 nm. Er^{3+}-doped glass has been widely used in a variety of optical applications, particularly in the area of glass safety lasers and optical amplifiers for optical fiber communications. Yb^{3+} ions have a strong transmission intensity in the near-infrared domain, a high quantum yield, and a relatively long fluorescence lifetime. In addition, due to the high absorption cross section of Yb^{3+} and the energy transfer process from Yb^{3+} to Er^{3+} ions, Yb^{3+}/Er^{3+} co-doping can enhance visible light up-conversion emission [5,6]. Among various possible host materials, phosphate glasses has excellent optical properties such as wide bandwidth emission spectrum, large diameter transmission window, high gain density and low up-conversion characteristics. Therefore, a great deal of research has been done on Yb^{3+} doped, Er^{3+} doped and Yb^{3+}/Er^{3+} co-doped phosphate, borosilicate and tellurite glasses.

In this study, doping of $50P_2O_5$–$30Sb_2O_3$–$10CaO$-$5Al_2O_3$–$5TeO_2$ glasses with Er_2O_3 and Yb_2O_3 were performed. The main research object is the influence of Yb^{3+} and Er^{3+} content on the spectral properties, structure and thermal properties of phosphate glass. The purpose of doping Yb^{3+} is to increase the absorption cross-section of the $^4I_{13/2}$–$^4I_{15/2}$ transition of Er^{3+}, and use the Judd–Ofelt (J-O) model to

* Corresponding author at: College of Materials Science and Engineering, Nanjing Tech University, Nanjing 210009, China.
E-mail address: zhang.512@njtech.edu.cn (Y. Zhang).

https://doi.org/10.1016/j.ceramint.2018.09.015
Received 25 July 2018; Received in revised form 16 August 2018; Accepted 2 September 2018
Available online 04 September 2018

examine its applicability as a potential optical glass laser and fiber amplifier.

2. Experimental methods

Glass samples were prepared by high temperature melting according to the following molar ratio, single doped sample $50P_2O_5$–$30Sb_2O_3$–10CaO-$5Al_2O_3$–$5TeO_2$-xEr_2O_3 (x = 0.25, 0.5, 0.75, 1, 2 mol%) and co-doped sample $50P_2O_5$–$30Sb_2O_3$–10CaO-$5Al_2O_3$–$5TeO_2$-$0.5Er_2O_3$-yYb_2O_3 (y = 1, 2, 3, 4, 5 mol%). The purity of all initial components exceeds 99.7%. All chemical reagents were ground in an agate mortar, poured into a platinum crucible, and melted at a temperature of 1100 °C for 1 h, then poured into a previously prepared mold, annealed, held in a furnace at 300 °C for 1 h, and then slowly cooled to obtain a glass sample. The resulting glass was carefully cut and polished to meet the optical measurement requirements.

Prepared glass sample was measured by X-ray diffraction (Geigerflex-Rigaku Japan) to determine the amorphous structure of the glass and the phase composition of the crystallized sample. The Archimedes method was used to determine the density of all samples. The molar volume formula is $V_m = M/\rho$, where M is the average molar mass of the glass and ρ is the measured glass density. A high temperature horizontal thermal dilatometer (PCY, Xiangtan Co., Ltd, China) was used to determine the coefficient of thermal expansion (CTE), glass transition temperature (T_g) and glass softening temperature (T_f) of the glass samples. The optical absorption spectra of glass samples were measured in the wavelength range of 300–1900 nm on a spectrophotometer UV–vis (Jasco-670 japan) The emission spectra of glass samples were taken in the wavelength range of 1400–1750 nm by a fluorescence spectrometer (FLS980 Britain) transition.

3. Results and discussions

3.1. XRD

The XRD pattern of single-doped and co-doped glass (Er0.25, Er0.5, Er0.5Yb1, Er0.5Yb3 Er0.5Yb4) are displayed in Fig. 1. As shown in Fig. 1, there are "amorphous peaks" with typical glass characteristics for doped samples with different contents of Er_2O_3, and there is no tendency for any crystallization, indicating that the doping of a small amount of Er_2O_3 does not cause crystallization of the glass. When the glass system is co-doped with Yb_2O_3 less than 3 mol%, the glass is completely transparent. It can be seen from Fig. 1 that the glass of Yb_2O_3 less than 3 mol% does not have any crystallization peak,

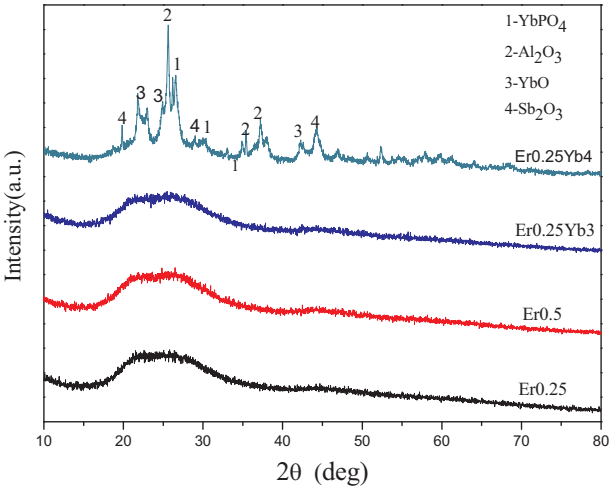

Fig. 1. X-ray diffraction patterns of Er0.25, Er0.5, Er0.5Yb1, Er0.5Yb3, Er0.5Yb4 glasses.

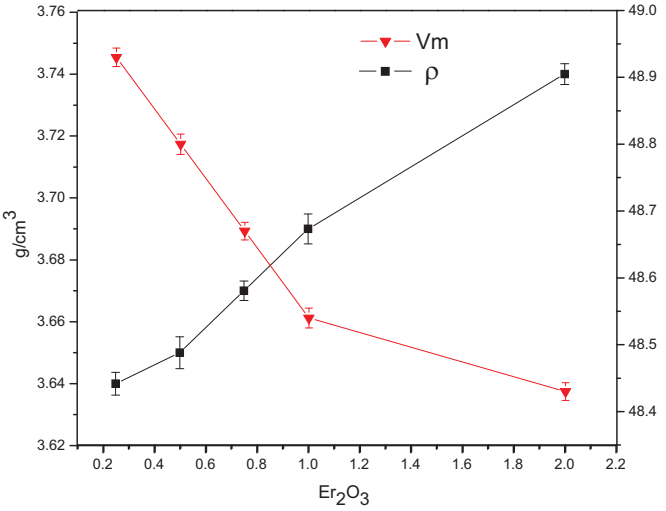

Fig. 2. The relationship of density, molar volume and composition of $50P_2O_5$–$30Sb_2O_3$–10CaO-5 Al_2O_3–$5TeO_2$ + xEr_2O_3 (x = 0.25, 0.5, 0.75, 1, 2) glasses.

indicating that the glass is not crystallized. When the content of Yb_2O_3 is 3 mol%, it can be seen that the glass is slightly milkiess. As can be seen from Fig. 1, the glass having a Yb_2O_3 content of 3 mol% does not have any crystallization peak, indicating that the glass is stratified without crystallization. When the content of Yb_2O_3 is 4 mol%, the glass is completely opaque. As can be seen from Fig. 1, the glass having a Yb_2O_3 content of 4 mol% has a distinct and sharp crystallization peak, indicating that the glass begins to crystallize. These precipitated crystals are: $YbPO_4$, Al_2O_3, YbO, Sb_2O_3.

3.2. Density and thermal properties

Fig. 2 is the relationship of density, molar volume and composition of $50P_2O_5$–$30Sb_2O_3$–10CaO-5 Al_2O_3–$5TeO_2$ + xEr_2O_3 (x = 0.25, 0.5, 0.75, 1, 2) glasses. It can be seen that the density of the glass gradually increases as the Er_2O_3 content increases. Because the relative molecular mass of Er_2O_3 is relatively larger, and the addition of a small amount of Er_2O_3 has little effect on the glass physical characteristics, the density of the glass increases with the increase of the content of Er_2O_3. Fig. 3 is the transition temperature (T_g), softening temperature (T_f) and coefficient of thermal expansion (CTE) of a glass sample. As shown in Fig. 3, as the content of Er_2O_3 increases, the T_g and T_f of the glass also gradually

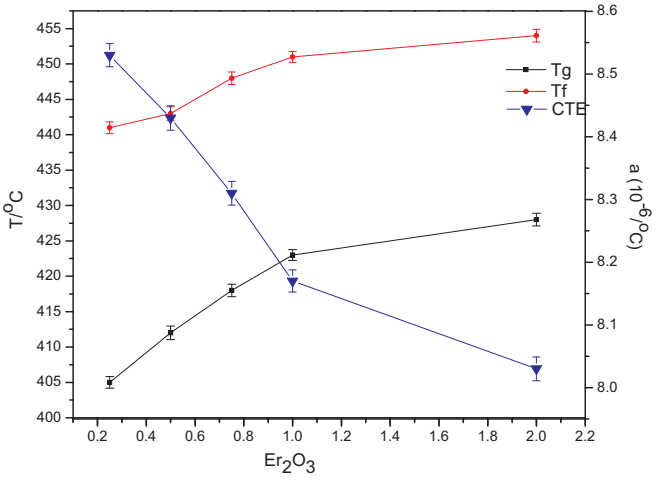

Fig. 3. The relationship of thermal properties (T_g, T_f, CTE) and composition of erbium-glasses.

increase. The thermal properties of the material depend on the composition and structure of the glass network. When the network structure of the glass becomes tight, the T_g and T_f are increased. When the melting temperature of the components in the glass network increases, T_g and T_f also rise. When the content of Er_2O_3 increases, the glass network becomes more compact, resulting in a decrease in the coefficient of thermal expansion of the glass system. Er_2O_3 can be used as a glass modification, and its effects on T_g, T_s and CTE are closely related to their field strength. The field strength (F), the binding ability of the modified cation and the non-bridged oxygen can be calculated by $F = Z_1Z_2e_2 / r_2$, where Z_1, Z_2 represent the valence of oxygen and cation, e represents the electron charge, and r represents the cation and the distance of oxygen ions. In general, the greater the field strength, the greater the network modification. Er^{3+} has a higher field strength and its stronger binding ability to non-bridged oxygen, thereby enhancing the network strength of phosphate. Therefore, as the Er^{3+} in the composition increases, it has a higher field strength, resulting in an increase in T_g, T_s, and a decrease in CTE.

3.3. FT-IR analyses

The FT-IR spectra provides information about the vibrations of various molecules and the rotation of covalent bonds in the network structure. We all know that the O/P ratio in phosphate glass has a great influence on its structure and properties. As the O/P ratio increases, the cross-linked Q^3 unit phosphate network depolymerizes (O/P = 2.5) in the linear Q^2 unit (O/P = 3), further depolymerizing into Q^1 units (O/P = 3.5), and finally into an isolated Q° unit (O/P = 4) [7].

Fig. 4 shows the FT-IR spectra of single-doped and co-doped glass. The FT-IR spectra indicated that the absorption peak at 522 cm^{-1} is formed by the overlap of two peaks of 480 cm^{-1} and 574 cm^{-1}, mainly due to the vibration mode of the $(PO_4)^{3-}$ group in the Q° unit and bending vibration of the O–P–O bond in the Q^1 unit [8]. The peak at 745 cm^{-1} is attributed to the symmetric stretching vibration of P–O–P bond [9], and the peak at 914 cm^{-1} is attributed to the asymmetric stretching vibration of the P–O–P bond [10]. There is a wide and large band at 1040 cm^{-1} due to the stretching vibration of the P-O tetrahedron. In addition, the peak at 1144 cm^{-1} is attributed to the antisymmetric stretching vibration of the O–P–O bond in the Q^1 unit. The band at 1385 cm^{-1} is considered to be a symmetric stretching vibration of the P=O bond. The absorption peak at 630 cm^{-1} is related to the presence of the P–O–Sb bond [11]. The position of the peak indicates the structural environment around the chemical bond. It can be seen from Fig. 4, there is no significant change in the position and intensity of the peaks with the change of Er_2O_3 and Yb_2O_3 content, which indicates that Er_2O_3 and Yb_2O_3 do not significantly affect the structure of the glass or the structure changes very small due to too little doping amount of rare earth.

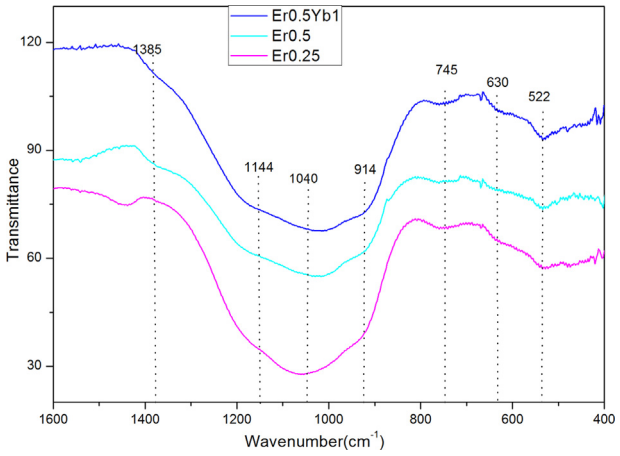

Fig. 4. The FT-IR spectra of Er0.25, Er0.5 and Er0.5Yb1 glasses.

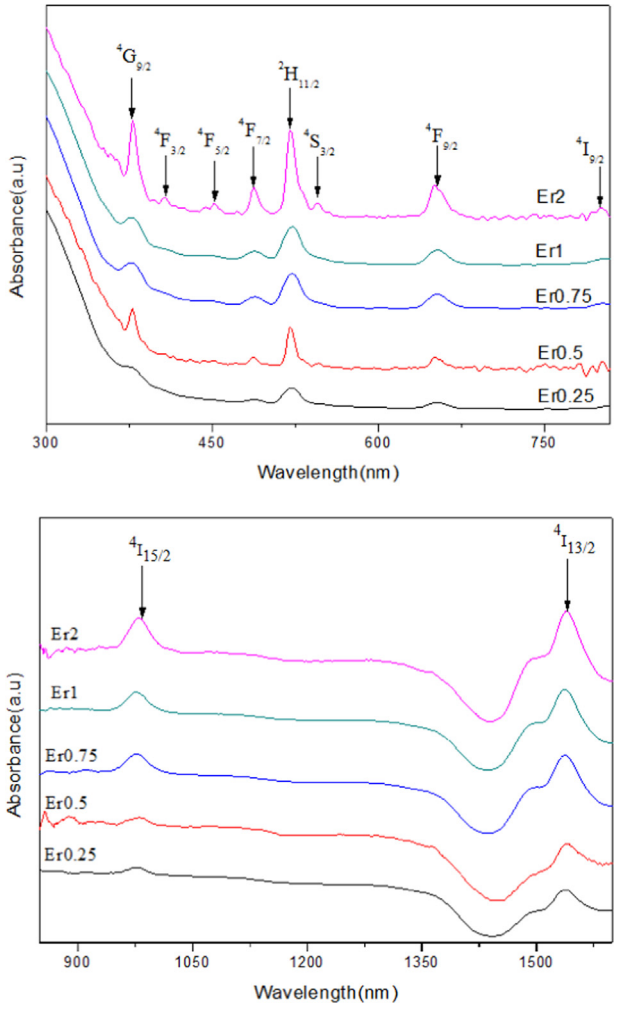

Fig. 5. Absorption spectra of Er^{3+} single doped phosphate glasses.

3.4. Absorption spectra

Fig. 5 shows the optical absorption spectra of a single doped Er^{3+} phosphate glass containing 10 absorption peaks at 1537, 976, 797, 651, 541, 520, 487, 450, 406 and 370 nm, respectively. Corresponding absorption from the ground state $^4I_{15/2}$ to the excited state $^4I_{13/2}$, $^4I_{11/2}$, $^4I_{9/2}$, $^4F_{9/2}$, $^4S_{3/2}$, $^4H_{11/2}$, $^4F_{7/2}$, $^4F_{5/2}$, $^4H_{9/2}$ and $^4G_{11/2}$, as shown in Fig. 5. It is found that all the absorption bands are the same for Er^{3+} single-doped and Yb^{3+}/ Er^{3+} co-doped glass except for some differences in the spectral bands. It can be seen from Fig. 6, Yb^{3+}/ Er^{3+} co-doped phosphate glass has broad and strong absorption of $^2F_{7/2} \rightarrow {}^2F_{5/2}$ at 976 nm, due to the large spectral overlap between Er^{3+} absorption ($^4I_{15/2} \rightarrow {}^4I_{11/\ 2}$) and Yb^{3+} emission ($^2F_{5/2} \rightarrow {}^2F_{7/2}$), so it has a strong absorption coefficient.

The J-O intensity parameter can be obtained by analyzing the absorption spectrum to predict the radiative transition probabilities, branching ratios, and radiation lifetimes for different transitions. Particularly, the value of the ground state to $^4I_{13/2}$ (1.55 μm) can be predicted using the Judd-Ofelt model. The absorption band within the experimental area determines the measured intensity of the absorption line of the induced dipole transitions in each band. The experimental line strength S_{exp} can be expressed by the following formula (1) [12]:

$$S_{exp}(J \rightarrow J') = \frac{3ch(2J+1)}{8\pi^3\lambda e^2 N_0}\left[\frac{9n}{(n^2+2)^2}\right]\int a(\lambda)d\lambda \quad (1)$$

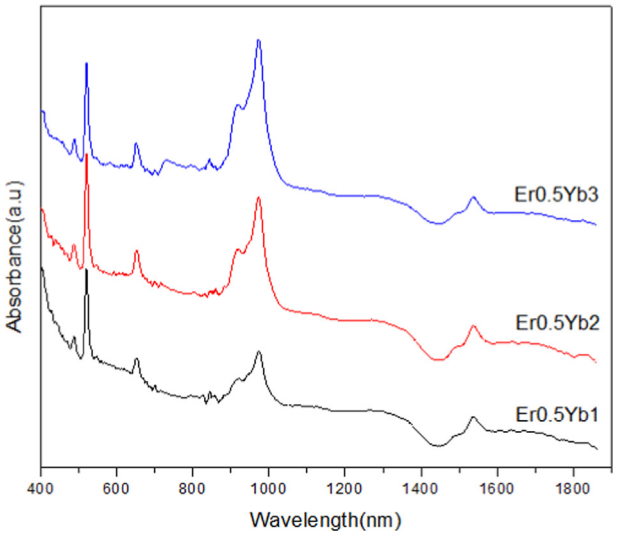

Fig. 6. Absorption spectra of $50P_2O_5$–$30Sb_2O_3$–10CaO-$5Al_2O_3$–$5TeO_2$–$0.5Er_2O_3$ + xYb_2O_3 (x = 1, 2, 3 mol) glasses.

where J and J' in the formula respectively are the number of initial and final states of the total angular momentum quantum, respectively. H is Planck's constant, C is the speed of light in vacuum, λ is the wavelength of each absorption band, e is the charge of electrons, N_0 is the concentration of Er^{3+} ions per unit volume, n is the refractive index at the relative wavelength and does not change with λ. The factor $[9n/(n^2 + 2)^2]$ in the formula is the local field correction of the ions in the dielectrics, $T = \int a(\lambda)d\lambda$ represents the integral absorption coefficient of λ.

The value of S_{exp} obtained by numerical integration of the shape of the absorption line was used to obtain the Judd-Ofelt parameter Ω_t, which is fitted using experimental data using the theoretical expressions of the Judd and Ofelt (2) [13].

$$S_{cal}(J \rightarrow J') = \sum_{t=2,4,6} \Omega_t |(S, L)J\|U^t\|(S', L')J'|^2 \quad (2)$$

where Ω_2, Ω_4, Ω_6 in the formula are the Judd-Ofelt parameter, $\|U^t\|$ (t = 2, 4 and 6) represents the bi-matrix of the unit tensor operator, which is derived from the state-characteristic quantum numbers (S, L, J) and (S', L', J') intermediate coupling approximate calculations. The elements of the matrix can be easily estimated from the data in the Nielson and Koster tables, and the matrix material has no effect on it [14,15]. The J parameters show the probability of matrix transfer because they contain crystal field parameters, radial integration between configurations, and interactions between the intermediate environment and the central ions [16,17].

When the three absorption peaks overlap, the square matrix element is summed from the matched square matrix elements in Table 1.

The average wavelength values of Er/Yb (0.5/0) and Er/Yb (0.5/1) glasses, The experimental line strengths (S_{exp}) and the calculated line strengths (S_{cal}) are shown in Table 2. The J-O strength parameter Ω_t (t = 2, 4, 6) is obtained using the least squares method by assuming $S_{exp} = S_{cal}$. The calculated line strengths can be evaluated by the root mean

Table 1
Values of the reduced matrix elements for the absorption transitions of Er^{3+}.

Transition from $^4I_{15/2}$ to	$(U^{(2)})^2$	$(U^{(4)})^2$	$(U^{(6)})^2$
$^4I_{13/2}$	0.0195	0.1173	1.4316
$^4I_{11/2}$	0.0282	0.0003	0.991
$^4F_{9/2}$	0.0	0.5354	0.4618
$^4H_{11/2}$	0.7125	0.4125	0.0925
$^4F_{7/2}$	0.0	0.1469	0.6266

Table 2
Values of the average wavelengths, experimental and calculated line strengths of Er/Yb(0.5/0) and Er/Yb(0.5/1) glasses.

Transition from $^4I_{15/2}$ to	λ_{abs} (nm)	S_{exp} (10^{-20} cm^2)	S_{cal} (10^{-20} cm^2)
$^4I_{13/2}$(Er/Yb(0.5/0))	1550	2.680	3.471
$^4I_{11/2}$	990	0.871	0.991
$^4F_{9/2}$	650	2.432	2.347
$^4H_{11/2}$	530	4.196	4.791
$^4F_{7/2}$	460	2.551	1.719
		$\Delta S_{rms} = 0.85 \times 10^{-20}$	
$^4I_{13/2}$ Er/Yb(0.5/1)	1550	3.567	3.491
$^4I_{11/2}$	990	1.046	2.351
$^4H_{11/2}$	530	4.406	4.599
$^4F_{7/2}$	460	1.603	1.648
$^4F_{9/2}$	650	2.013	1.943
		$\Delta S_{rms} = 0.74 \times 10^{-20}$	

square deviation ΔSrms, which is calculated using the following expression (3) [18]:

$$\Delta S_{rms} = [(q - p)^{-1} \sum (S_{exp} - S_{cal})^2]^2 \quad (3)$$

Here q and p are the number of analysis bands and the number of parameters, respectively. Here p is 3. The ΔS_{rms} values of Er0.5Yb0 and Er0.5Yb1 are very small, which are 0.85×10^{-20} and 0.74×10^{-20}, respectively. This indicates that the experimental line strength and the theoretical line strength fit well, and this experiment can be applied to the J-O theory.

Table 3 shows the Judd-Ofelt parameters (Ω_2, Ω_4, Ω_6) and the factor $\chi = \Omega_4/\Omega_6$ at different Yb^{3+} concentrations. All Ω_t (t = 2, 4, 6) parameters exhibit monotonic changes with low sensitivity to changes in Er^{3+} ions. However, the concentration of Yb^{3+} causes a significant change in the value of the Ω_t parameter. These phenomena prove that the concentration of Yb^{3+} affects the environment around Er^{3+}. At same time, Table 3 shows the comparison of J-O strength parameters (Ω_2, Ω_4, Ω_6) in different glass matrices. Based on the Jacobs and Weber theory [19,20], the Ω_4 and Ω_6 parameters can be used to describe Er^{3+} luminescence. Therefore, Ω_4/Ω_6 can be used to represent the spectral quality factor χ. If its parameter value is small, it indicates that the laser conversion $^4I_{13/2}$–$^4I_{15/2}$ is strong. When the Er^{3+} in the phosphate glass is 0.5 mol% and the Yb^{3+} is 3 mol%, this parameter is 0.48. The spectral quality factors χ are very important in predicting the various laser transition behaviors of a given organization matrix. In this work, χ decreased as the content of rare earth ions increased. It should be noted here that the presence of Yb^{3+} as a sensitizer reduces the quality factor. It is shown to be very important in the fluorescence kinetics of the Yb^{3+}/Er^{3+} co-doped system. The lower spectral quality factor indicates that the phosphate glass of this system has a promising future in rare earth-doped transparent optical glass, which can be applied to glass lasers and amplifiers.

The spectral intensity of each transition can be obtained by the calculation of the J-O intensity parameter, and then the spectral intensity is used to calculate the spontaneous transition probability (A_{rad}), the radiation lifetime (τ_{rad}) and the branching ratio ($\beta_{JJ'}$) of each corresponding transition. The calculation expression are as follows (4):

$$A_{rad}[J, \quad J'] = \frac{64\pi^4 e^2}{3h(2J+1)\pi^3} \times [\chi_{ed} Sed + \chi_{md} S_{md}] \quad (4)$$

Table 3
Judd–Ofelt parameters of the erbium in different host materials.

Host materials	Ω_2	Ω_4	Ω_6	$\chi = \Omega_4/\Omega_6$
Er/Yb(0.5/0)	4.98	2.53	2.15	1.18
Er/Yb(0.5/1)	4.98	1.71	2.23	0.77
Er/Yb(0.5/2)	5.13	1.32	2.16	0.61
Er/Yb(0.5/3)	5.32	0.98	2.04	0.48

The experimental line strengths are the sum of the electrical dipole transitions (S_{ed}) and the magnetic dipole transitions (S_{md}). In the theoretical calculation, only the electrical dipole transitions are involved, so if there is a magnetic dipole transition, then the intensity of this part should be subtracted. The formula is as follows (5) and (6):

$$S_{exp} = S_{ed} + S_{md} \tag{5}$$

$$S_{md} = \frac{1}{4m^2c^2}|\langle (S, \quad L)J\|L+2S\|(S', L')\rangle|^2 \tag{6}$$

It can be seen from the formula that if there is a magnetic dipole transition, the magnetic dipole transition strength is independent of the nature of the rare earth ion matrix, so the common magnetic dipole transition strength can be queried by the literature.

The formula for calculating the radiation lifetime (τ_{rad}) is as follows (7):

$$\tau_{rad} = \left\{ \sum_{S',L',J'} A_{rad}|(S, L)J;(S', L')J'| \right\}^{-1} \tag{7}$$

The fluorescence branching ratio ($\beta_{JJ'}$) can be used as a useful parameter for predicting laser performance. Its expression is as follows (8):

$$\beta_{JJ'}[(S, L)J;(S',L')J'] = \frac{A[(S, L)J;(S',L')J']}{\sum_{S',L',J'} A[(S, L)J;(S',L')J']} \tag{8}$$

Table 4 shows the calculated values of A_{rad}, τ_{rad} and $\beta_{JJ'}$ for the Er0.5 and Er0.5Yb1 doped glass samples. This indicates that the Er0.5-doped glass has a lower radiation lifetime than the Er0.5Yb1-doped glass sample, demonstrating that there is an efficient energy transfer between Yb^{3+} and Er^{3+}.

3.5. Emission spectra at room temperature

Fig. 7 shows the emission spectrum of the Er^{3+}/Yb^{3+} co-doped phosphate glass in the 1400–1750 nm wavelength range at 980 nm excitation. The emission spectrum shows the effect of Yb^{3+} concentration on the radiation intensity. There is a distinctly broad emission band at 1564 nm (1.56 μm), which corresponds to the transition of the $^4I_{13/2}$–$^4I_{15/2}$ energy level of Er^{3+}. When the concentration of Er^{3+} is less than 0.5 mol%, the transition intensity of $^4I_{13/2}$–$^4I_{15/2}$ increases with the increase of Er^{3+}. When the concentration is greater than 0.5 mol%, the transition intensity decreases with the increase of Er^{3+} due to the photo quenching effect. The quenching of light is mutual, and non-radiative energy conversion is included in the Er^{3+} doping. This phenomenon can also be called the self-concentration quenching, because at high concentrations of Er^{3+}, the interaction is very strong due to the small ion spacing, which leads to the formation of ion clusters and non-radiative processes, thereby increasing the non-radiative rate to cause luminescence quenching [21]. In addition, the gradually increasing concentration quenching effect will result in weaker emission intensity. Fig. 7 shows that the emission intensity of the co-doped sample is much greater than the emission intensity of the single-doped sample, indicating the effective energy transfer between Yb^{3+} and Er^{3+}. Initially, Yb^{3+} excited from $^2F_{7/2}$ ground state to $^2F_{5/2}$ under 980 nm laser excitation. Under this condition, Yb^{3+} doping is a photosensitizer and energy transmitter for Er^{3+} in the $^4I_{15/2}$ ground state. After the energy is absorbed, Er^{3+} is excited to $^4I_{11/2}$, and then the non-radiative decay [$^4I_{11/2}$ - $^4I_{13/2}$ (Er^{3+})] occurs rapidly, causing $^4I_{13/2}$ to become metastable. In addition, the $^4I_{11/2}$ excited state of Er^{3+} is similar to the Yb^{3+} excited state [22,23]. The energy transfer mechanism described above is shown in Fig. 8.

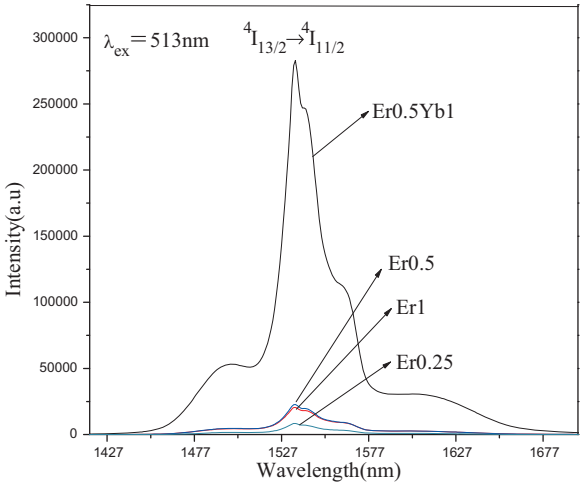

Fig. 7. Emission spectra of Er^{3+} doped and Er^{3+}/Yb^{3+}-codoped glasses.

These factors facilitate the energy transfer process and increase the luminescence intensity of the doped glass. Here, the J-O intensity parameter is used to determine the important radiation characteristics in the $^4I_{13/2}$–$^4I_{15/2}$ transition, such as λ_p, A_{rad}, σ_e, $\Delta\lambda_p$, and $\beta_{JJ'}$.

For optical fiber amplifiers, the effective bandwidth is a very important parameter. The synergistic effect of the local structure and the ions surrounding of the Er^{3+} in this glass sample is an important factor in the enlargement of the luminescent band. Normally, non-homogeneous expansion of Er^{3+} is dominant in glass. This widening of the bandwidth is due to re-absorption/self-absorption, which usually causes the absorption and emission spectra to overlap in the ternary systems [24].

The change of Δλp in the glass doped with different concentrations of Yb^{3+} is very significant, which proves that the change of the

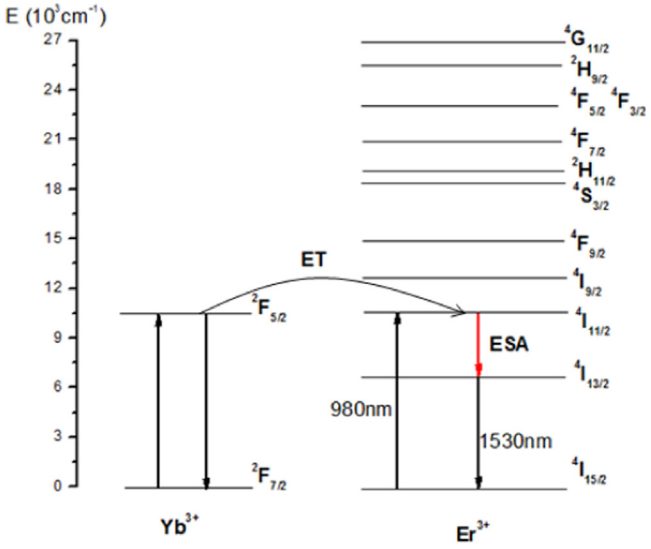

Fig. 8. Energy level diagram of Er0.5Yb1 glass.

Table 4
Radiative properties of $^4I_{13/2}$–$^4I_{15/2}$ transitions in Er^{3+} doped and Er^{3+}-Yb^{3+} co-doped phosphate glasses.

Radiative properties	Er0.5	Er0.5Yb1
Peak emission wavelength (λ_p, nm)	1560	1560
Effective linewidth ($\Delta\lambda_p$, nm)	106	183
Radiative transition probability (A_{rad}, s^{-1})	152	743
Fluorescence branching ratio ($\beta_{JJ'}$)	1	1
Stimulated emission cross section (σ_e, 10^{-20} cm^2)	0.51	2.68
Gain band width ($\sigma_e \times \Delta\lambda_p$, 10^{-25} cm^3)	0.54	2.74
Optical gain parameter ($\sigma_e \times \tau_{rad}$, 10^{-25} cm^2 s)	186.51	271.28
Radiative lifetime (τ_{rad}, ms)	4.62	1.24

coordination field of Er^{3+} is affected by the doping of Yb^{3+}, resulting in the non-uniform broadening of the emission spectrum. Besides, the full width at half maximum ($\Delta\lambda_P$) of the Er0.5 and Er0.5Yb1 glasses is 106 nm and 183 nm, which is very large for the application of wavelength division multiplexing (WDM). The larger $\Delta\lambda_P$ value is extremely helpful in WDM applications [25]. For the application of the amplifier, the importance of the stimulated emission cross section in the conversion is second only to the line width. Therefore, σ_e and $\Delta\lambda_P$ are extremely useful parameters in achieving bandwidth, high-gain amplification in optical amplifiers. The radiation-induced transition can be enhanced by doping with Yb^{3+}, which will significantly increase the values of σ_e and $\Delta\lambda_P$. The optical gain is evaluated by analyzing the bandwidth gain ($\sigma_e \times \Delta\lambda_P$) and optical gain ($\sigma_e \times \tau_{rad}$) of the optical amplifier. Large bandwidth and optical gain are required for the optical amplifier, because the energy bandwidth is lower for large bandwidths [26]. Table 4 shows the calculation of the radiation and the optical properties of the Er0.5 and Er0.5Yb1 glass samples. These values indicate that this glass can be well applied in the manufacture of fiber amplifiers because of its greater τ_{rad}, σ_e, and $\Delta\lambda_P$ values than the reported glass [27,28]. Therefore, this glass is a good carrier for doping Er^{3+} and Yb^{3+}.

4. Conclusions

Rare earth doped phosphate glasses ($50P_2O_5$–$30Sb_2O_3$–$10CaO$-$5Al_2O_3$–$5TeO_2$-xEr_2O_3-yYb_2O_3) was successfully prepared by high temperature melting method. It is found that when the glass system is doped with more than 3 mol% of Yb_2O_3, some crystals will precipitate in the glass. The Judd-Ofelt parameters of Ω_t (t = 2, 4, 6) are largely sensitive to the codoping of Yb^{3+}, and the spectral quality factor χ decreases with Yb_2O_3 doping. At the same time, Yb^{3+}/ Er^{3+} co-doping results in an increase in the emission intensity of $^4I_{13/2}$–$^4I_{15/2}$, which showed an effective energy transfer between Yb^{3+} and Er^{3+}. The optical properties of Er^{3+}/Yb^{3+} co-doped phosphate glasses were comprehensively studied and analyzed using the radiative transition probabilities (A_{rad}), stimulated emission cross sections (σ_e), branching ratios ($\beta_{JJ'}$), maximum half-width values ($\Delta\lambda_p$), and the radiation lifetime (τ_{rad}) of the glass. The comprehensive research results indicate that Er^{3+}/Yb^{3+} co-doped phosphate glass has great application prospects in solid-state NIR lasers and fiber amplifiers.

Acknowledgments

This work was financially supported by the Priority Academic Program Development of Jiangsu Higher Education Institutions and Jiangsu Collaborative Innovation Center For Advanced Inorganic Function Composites.

References

[1] Y.C. Xu, S.G. Li, L.L. Hu, W. Chen, Effect of copper impurity on the optical loss and Nd^{3+} nonradiative energy loss of Nd-doped phosphate laser glass, J. Rare Earth 29 (6) (2011) 614–621.
[2] M.I. Abdel-Ati, A.A. Higazy, Electrical conductivity andoptical properties of gamma-irradiated niobium phosphateglasses, J. Mater. Sci. 35 (2000) 6175.
[3] R. Praveena, V. Venkatramu, P. Babu, C.K. Jayasankar, Fluorescence spectroscopy of Sm^{3+} ions in P_2O_5-PbO-Nb_2O_5 glasses, Physica B 40 (3) (2008) 3527.
[4] A. Biswas, G.S. Maciel, C.S. Friend, Upconversion properties of a transparent Er^{3+}–Yb^{3+} co-doped LaF3-SiO2 glass-ceramics prepared by sol-gel method, J. Non-Cryst. Solids 31 (6) (2003) 393–397.
[5] F.Y. Weng, D.Q. Chen, Y.S. Wang, H. Lin, Energy transfer and up-conversion luminescence in Er^{3+}/Yb^{3+}co- doped transparent glass ceramic containing YF_3 nanocrystals, Ceram. Int. (2009).
[6] C.W. Nielson, G.F. Koster, Spectroscopic Coefficients for pn, dn and fn Configurations, MIT Press, Cambridge. MA, 1964.
[7] G. Walter, U. Hoppe, J. Vogel, Harmann, The structure of zinc polyphosphate glass studied by diffraction methods and P-31 NMR, J. Non-Cryst. Solids 33 (3) (2004) 252–262.
[8] P.Y. Shih, Properties and FTIR spectra of lead phosphate glasses for nuclear waste immobilization, Mater. Chem. Phys. (2003) 299–304.
[9] D.A. Magdas, N.S. Vedeanu, D. Toloman, Study on the effect of vanadium oxide in calcium phosphate glasses by Raman, IR and UV–vis spectroscopy, J. Non-Cryst. Solids 42 (8) (2015) 151–155.
[10] C. Dayanand, G. Bhikshamaiah, V.J. Tyagaraju, Structural investigations of phosphate glasses: a detailed infrared study of the x (PbO)-(1 − x) P_2O_5 vitreous system, J. Mater. Sci. 31 (1996) 1945–1967.
[11] B. Zhang, Q. Chen, L. Song, The influence of Sb_2O_3 addition on the properties of low-melting ZnO-P2O5 glasses, J. Am. Ceram. Soc. 91 (2008) 2036–2038.
[12] H. Desirena, E. De la Rosa, L.A. Díaz-Torres, Concentration effect of Er^{3+} ion on the spectroscopic properties of Er^{3+} and Yb^{3+}/Er^{3+} co-doped phosphate glasses, Opt. Mater. 28 (2006) 560–567.
[13] E.O. Serqueira, N.O. Dantas, A.F.G. Monte, M.J.V. Bell, Judd Ofelt calculation of quantum efficiencies and branching ratios of Nd^{3+} doped glasses, J. Non-Cryst. Solids 35 (2) (2006) 3628–3632.
[14] W.T. Carnall, P.R. Fields, K. Rajnak, Spectral intensities of the trivalent lanthanides and actinides in solution. II. Pm^{3+}, Sm^{3+}, Eu3+, Gd^{3+}, Tb^{3+}, Dy^{3+} and Ho^{3+}, J. Chem. Phys. 49 (1968) 4412–4423.
[15] Q.Y. Zhang, Z.M. Feng, Z.M. Yang, Z.H. Jiang, Energy transfer and infrared to-visible upconversion luminescence of Er^{3+}/Yb^{3+}-codoped halide modified tellurite glasses, J. Quant. Spectrosc. Radiat. 98 (2006) 167–179.
[16] W.T. Carnall, P.R. Fields, R. Rajnak, Electronic energy levels in the trivalent lanthanide aquo ions. I. Pr3+, Nd3+, Pm3+, Sm^{3+}, Dy^{3+}, Ho^{3+}, $Er^{3+}$and Tm^{3+}, J. Chem. Phys. 49 (1968) 4424–4442.
[17] S. Tanabe, Optical transitions of rare earth ions for amplifiers: how the local structure works in glass, J. Non-Cryst. Solids 25 (9) (1999) 1–9.
[18] Y. Nageno, H. Takebe, K. Morinaga, Correlation between radiative transition-probabilities of Nd^{3+} and composition in silicate, borate, and phosphate glasses, J. Am. Ceram. Soc. 76 (1993) 3081–3086.
[19] N. Sdiri, H. Elhouichet, C. Barthou, M. Ferid, Spectroscopic properties of Er^{3+} and Yb^{3+} doped phosphate–borate glasses, J. Mol. Struct. 1010 (2012) 85–90.
[20] I. Jlassi, H. Elhouichet, M. Ferid, C. Barthou, Judd–Ofelt analysis and improvement of thermal and optical properties of tellurite glasses by adding P2O5, J. Lumin. 130 (2010) 2394–2401.
[21] Y. Tian, R. Xu, L. Zhang, L. Hu, J. Zhang, Observation of 2.7 μm emission from diode-pumped Er^{3+}/Pr^{3+}-codoped fluorophosphate glass, Opt. Lett. 36 (2011) 109–111.
[22] Y. Tian, R. Xu, L. Hu, J. Zhang, Spectroscopic properties and energy transfer process in Er^{3+} doped ZrF4-based fluoride glass for 2.7 μm laser materials, Opt. Mater. 34 (2011) 308–312.
[23] H. Lin, D. Chen, Y. Yu, A. Yang, Y. Wang, Enhanced mid-infrared emissions of Er^{3+} at 2.7 mm via Nd^{3+} sensitization in chalcohalide glass, Opt. Lett. 36 (2011) 1815–1817.
[24] D.K. Sardar, W.M. Bradley, J.J. Perez, J.B. Gruber, J.A. Hutchinson, C.W. Trussell, M.R. Kokta, Judd–Ofelt analysis of the Er^{3+} (4f11) absorption intensities in Er^{3+}-doped garnets, J. Appl. Phys. 93 (2003) 2602–2607.
[25] D. Ramachari, L. Rama Moorthy, C.K. Jayasankar, Gain properties and concentration quenching of Er^{3+}-doped niobium oxyfluorosilicate glasses for photonic applications, Opt. Mater. 36 (2014) 823–828.
[26] B.C. Jamalaiah, T. Suhasini, L. Rama Moorthy, K. Janardhan Reddy, I.I.-Gon Kim, Dong-Sun Yoo, Kiwan Jang, Visible and near infrared luminescence properties of Er^{3+}-doped LBTAF glasses for optical amplifiers, Opt. Mater. 34 (2012) 81–867.
[27] Y. Yang, Z. Yang, B. Chen, et al., Spectroscopic properties and thermal stability of Er^{3+} -doped germinate-borate glasses, J. Alloy. Compd. 47 (9) (2009) 883–887.
[28] N. Jaba, H.B. Mansour, B. Champagnon, The origin of spectral broadening of 1.53 μm emission in Er-doped zinc tellurite glass, Opt. Mater. 31 (2009) 1242–1247.